AGU PUBLICATIONS

Geophysical Research Letters

RESEARCH LETTER
10.1002/2016GL067812

Key Points:
- A new mixing mechanism induced by the interaction of internal bores and vertically sheared flow
- The Iribarren number plays a major role in the mixing intensity due to internal wave breaking
- The Iribarren number separates canonical bores from noncanonical bores

Correspondence to:
H. Yamazaki,
hide@kaiyodai.ac.jp

Citation:
Masunaga, E., O. B. Fringer, H. Yamazaki, and K. Amakasu (2016), Strong turbulent mixing induced by internal bores interacting with internal tide-driven vertically sheared flow, *Geophys. Res. Lett.*, *43*, doi:10.1002/2016GL067812.

Received 19 JAN 2016
Accepted 10 FEB 2016
Accepted article online 12 FEB 2016

Strong turbulent mixing induced by internal bores interacting with internal tide-driven vertically sheared flow

Eiji Masunaga[1], Oliver B. Fringer[2], Hidekatsu Yamazaki[1], and Kazuo Amakasu[3]

[1]Department of Ocean Sciences, Tokyo University of Marine Science and Technology, Tokyo, Japan, [2]Department of Civil and Environmental Engineering, Stanford University, Stanford, California, USA, [3]Research Center for Advanced Science and Technology, Tokyo University of Marine Science and Technology, Tokyo, Japan

Abstract We observed the formation of an internal bore interacting with the vertically sheared flow generated during the previous phase of the internal tide, which resulted in strong turbulent mixing. The rate of turbulent kinetic energy dissipation reached on the order of 10^{-5} W kg^{-1} during the event. Numerical simulations reproduced the observed interaction of internal bores with the sheared flow and verified the hypothesized breaking and mixing mechanism. The numerical results indicated that the Iribarren number, or the ratio of the topographic slope to the internal wave slope, plays a major role in the mixing intensity and types of internal bores. It was found that waves with low Iribarren numbers lead to bores that interact with vertically sheared flows induced by the previous phase of the internal tide and are more likely to produce strong wave breaking and mixing.

1. Introduction

Vertical turbulent mixing of heat and salt in the ocean is essential to maintaining the global ocean circulation [*Munk and Wunsch*, 1998; *St. Laurent and Thurnherr*, 2007]. Transport of nutrients and dissolved gases by turbulent mixing has been recognized as an important contributor to ocean ecosystem health and the global carbon cycle [*Walsh*, 1991; *Nakatsuka et al.*, 2004; *Sharples et al.*, 2009]. One important driver of ocean mixing is thought to be breaking of internal gravity waves [e.g., *MacKinnon and Gregg*, 2003; *Venayagamoorthy and Fringer*, 2006]. Recent studies suggest that continental shelves and shallow slopes are "hot spots" of internal wave breaking [*Cacchione et al.*, 2002; *Carter and Gregg*, 2002].

Energetic internal waves in coastal oceans are ubiquitous phenomena and can induce large isopycnal displacement [e.g., *Broenkow and McKain*, 1972], strong currents [e.g., *Van Gastel et al.*, 2009], sediment transport [e.g., *Cacchione et al.*, 2002], and turbulent mixing [e.g., *MacKinnon and Gregg*, 2003]. Shoaling internal tides run up on shallow coastal slopes and form highly nonlinear internal waves that are commonly referred to as internal "boluses" or "bores" [*Helfrich*, 1992]. Like surface waves, shoaling internal waves break, which leads to strong turbulent mixing events in coastal areas [e.g.,*Walter et al.*, 2012; *Masunaga et al.*, 2015].

Although the importance of internal waves for transport and mixing in the ocean is well known, details of internal wave breaking and mixing processes remain poorly understood owing to the difficulty of measuring such phenomena. Motivated by the lack of understanding of internal wave breaking and associated mixing in the literature, we conducted field surveys in Otsuchi Bay, Japan. In this study, we present an internal wave-breaking mechanism resulting from the interaction of vertically sheared flow due to an internal tide with a bore that develops during the subsequent phase of the internal tide.

2. Observations

2.1. Field Surveys

We carried out field surveys in Otsuchi Bay, Japan (Figure 1) on 10 September 2013. Two types of tow-yo instruments were deployed for transect observations, namely, the YODA Profiler [*Masunaga and Yamazaki*, 2014] and the Underway CTD (UCTD) [*Rudnick and Klinke*, 2007]. Observations were obtained from 5 m to 120 m depth over a distance of approximately 12 km. The YODA Profiler carries conductivity, temperature, depth, fluorescence, turbidity, and dissolved oxygen sensors. The UCTD carries conductivity, temperature, and depth sensors. The YODA Profiler was used to observe near-shore regions (depth $<$ 50 m), and the UCTD was used to observe

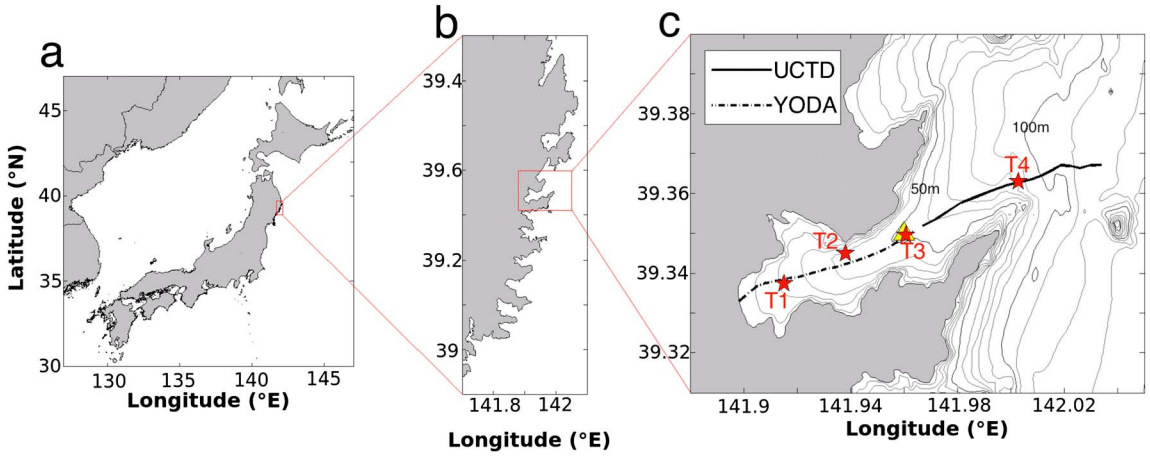

Figure 1. Field campaign site. Maps of (a) Japan, (b) the Sanriku Coast and (c) Ostuchi Bay. Black solid and dashed lines are the UCTD and the YODA Profiler transects, respectively. Red stars (T1–T4) indicate observation sites for the microstructure profiler TurboMAP-L. The yellow triangle (near T3) indicates the mooring location.

deeper areas (depth > 50 m). The YODA Profiler was deployed from the R/V *Grand-maillet* (the University of Tokyo), and the UCTD was deployed from the fishing vessel *Daini-wakashio-maru* (Kamaishi-Toubu fishery). The transect line was set up from the western end of the bay to its mouth at the ocean, and the total length of the transect between the two instruments was approximately 12 km (Figure 1). The sinking velocity of the YODA Profiler and UCTD were adjusted to be 0.5 m s^{-1} and 3 m s^{-1}, respectively. The YODA Profiler and UCTD recorded data at 10 Hz and 16 Hz sampling frequencies, respectively. In order to estimate the rate of turbulent kinetic energy dissipation, the microstructure profiler, TurboMAP-L [*Doubell et al.*, 2009], was deployed at four locations (T1–T4, Figure 1c) from the same vessel as the UCTD survey. A multifrequency echo sounder, Acoustic Zooplankton Fish Profiler [*Lemon et al.*, 2012], was mounted downward on the R/V *Grand-maillet* during the survey and recorded data at 1 Hz with 3.75×10^{-2} m vertical resolution.

In addition to transect and microstructure surveys, we deployed a mooring system at the mouth of the bay between 10 June 2013 and 13 September 2013. This mooring location is shown in Figure 1. The mooring consisted of a thermistor chain and an upward looking 600 kHz acoustic Doppler current profiler. Details of this mooring system can be found in *Masunaga et al.* [2015].

2.2. Estimation of the Rate of Turbulent Kinetic Energy Dissipation

The rate of turbulent kinetic energy dissipation from TurboMAP-L was estimated with the isotropic formula

$$\varepsilon = 7.5\nu\overline{\left(\frac{du'}{dz}\right)^2}, \tag{1}$$

where u' is the horizontal component of turbulent velocity from a shear probe and ν is the kinematic viscosity of water. The rate of turbulent kinetic energy dissipation is also inferred using a statistical method described in *Masunaga and Yamazaki* [2014]. To infer the dissipation rate from the YODA Profiler, ε_C, we assumed the dissipation rate followed

$$\varepsilon_C = a\left[\overline{(dC/dz)^2}\right]^b, \tag{2}$$

where the coefficients $a = 6.5 \times 10^{-7}$ and $b = 1.26$ were obtained with a QQ plot (quantile versus quantile) comparing probability density functions of ε from TurboMAP-L and the variance of dC/dz from the YODA Profiler. Although this estimation method is an indirect turbulent measurement, the dissipation rate gives a reasonable approximation, at least to the correct order of magnitude [*Masunaga and Yamazaki*, 2014; *Masunaga et al.*, 2015].

2.3. Observed Results

Observed mooring data show that internal bores run up repeatedly on the slope in the bay (Figure 2a). Internal tides (internal waves of tidal frequency) are generated at the continental shelf break a few hundred

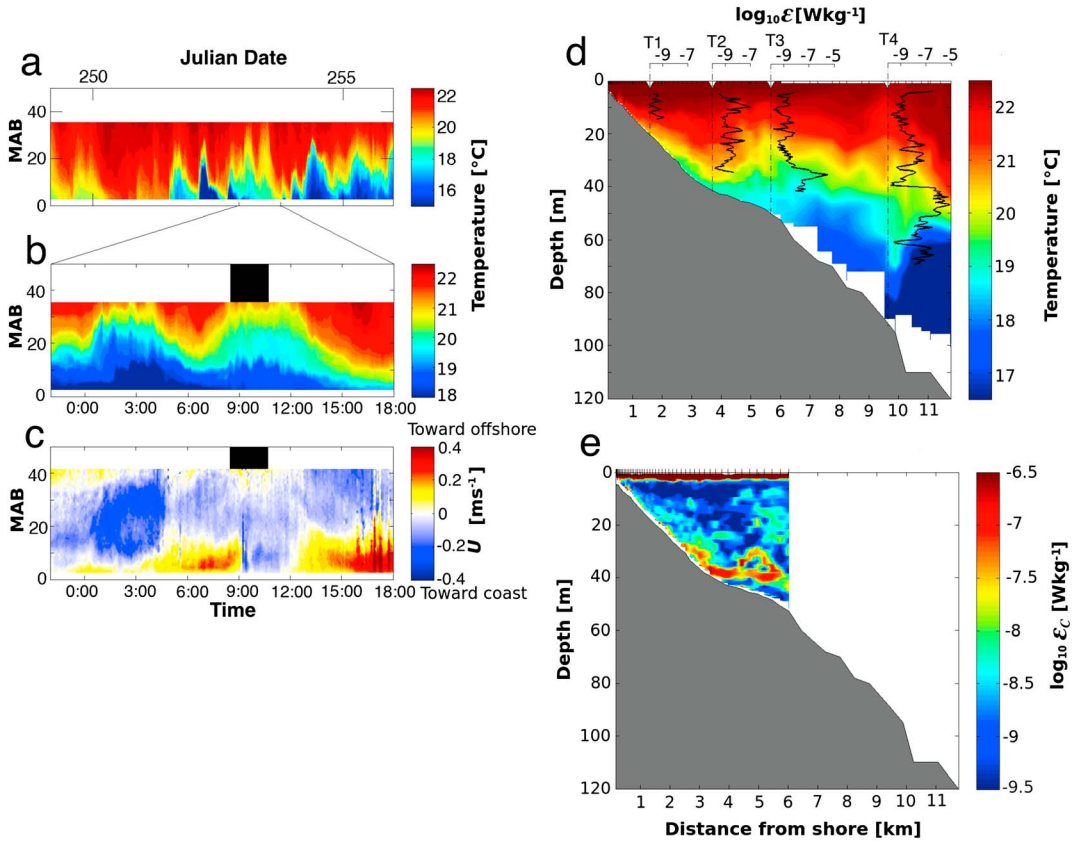

Figure 2. Observation results. Mooring data of (a, b) temperature and (c) cross-shore velocity, (d) temperature distribution from the YODA Profiler and the UCTD, (e) ε_C distribution estimated from the YODA Profiler survey. Black shaded areas in Figures 2b and 2c show the period of the transect observations. MAB represents meters above the bottom. Black lines drawn over temperature distribution in Figure 2d correspond to profiles of ε estimated from TurboMAP-L.

kilometers to the east of the Japanese coast [*Masunaga et al.*, 2015]. These waves propagate to the west from the shelf break and enter the mouth of Otsushi Bay where they form nonlinear bores that repeatedly run up the slope of the bay at tidal frequencies [*Masunaga et al.*, 2015]. As shown by the velocity data obtained from the moorings (Figure 2c), after the formation and upslope propagation of the bore associated with the first half, or crest, of an incident internal wave (Figures 2b and 2c, time = 9:00–12:00), the second half, or trough, produces vertical shear accompanied by strong downslope currents on the slope (Figures 2b and 2c, time = 6:00–9:00 and 12:00–18:00), reaching 0.4 m s^{-1}. With our field survey we observed the interaction of this vertically sheared flow with an upslope propagating bore. The YODA Profiler and the UCTD observations were made during the transition period in the internal tide that occurred between the strong downslope current phase of the internal tide and the bore runup phase when bottom currents switched from being directed offshore to onshore (Figure 2c, time ~ 9:00). Figure 2d shows the temperature distribution when the upslope propagating bore interacted with the strong shear flow accompanied by strong downslope flowing cold water (distance ~ 5 km). In addition to the large-scale runup bore, small-scale internal waves appeared behind the bore head (distance = 5–11 km).

The rate of turbulent kinetic energy dissipation, ε, estimated from TurboMAP-L showed high turbulent dissipation near the head of the bore (T3), reaching 2×10^{-6} W kg^{-1} (Figure 2d). The strong turbulent layer also appeared behind the bore head (T4), and the dissipation rate reached 8×10^{-6} W kg^{-1} (Figure 2d), which is approximately 10^4 times higher than the background turbulent intensity. This turbulent layer was located at middepth and had a thickness of approximately 20 m. Away from the bore-related mixing region, such as in the inner bay (T1), ε was low and in the range 10^{-10}–10^{-9} W kg^{-1}. The rate of turbulent kinetic energy dissipation estimated from the YODA Profiler elucidates details of the distribution of mixing within the breaking event (Figure 2e). Regions of high ε appeared in the bottom boundary layer (distance = 1–3.5 km)

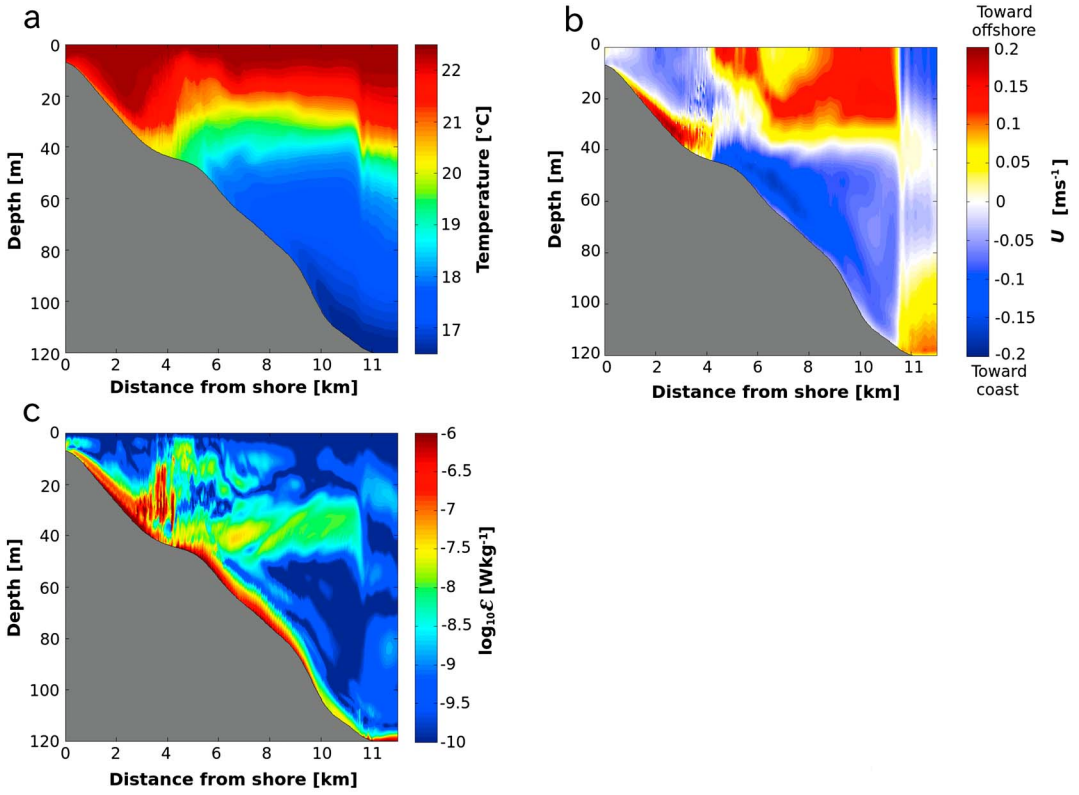

Figure 3. Numerical simulation results from the SUNTANS model, showing distributions of (a) temperature, (b) horizontal flow speed, and (c) the rate of turbulent kinetic energy dissipation.

and the head of the bore (distance = 3.5–6 km). The high dissipation in the turbulent layer in the downslope flowing cold water (distance = 1–3.5 km) is due to bottom boundary layer turbulence [*Dewey and Crawford*, 1988]. However, around the head of the bore at middepth, the region of strong turbulence was detached from the bottom and ε was much higher (Figures 2d and 2e, distance $>$ 4 km). Furthermore, the region of high dissipation extended close to the sea surface (Figure 2e, distance ~ 5 km). As it was detached from the bottom boundary, this turbulent region was likely generated by strong wave breaking due to the interaction of the vertically sheared flow and the incident bore.

3. Numerical Simulations

3.1. Numerical Simulations for Otsuchi Bay

In order to investigate the details of the physical processes associated with the observed internal bores in Otsuchi Bay, we used the nonlinear and nonhydrostatic SUNTANS model [*Fringer et al.*, 2006]. The domain length was 20 km with a slope similar to Otsuchi Bay and maximum depth of 120 m. The horizontal grid spacing was 20 m and the time step size was 1 s for all simulations. The vertical grid spacing was uniform in the vertical and set to 0.80 m. The model was initialized with temperature and salinity data taken from field surveys in Otsuchi Bay and was assumed to be horizontally uniform. The ocean boundary was forced with the first-mode baroclinic internal wave velocity field at the M_2 semidiurnal tidal frequency (see *Masunaga et al.* [2015] for more details). No heat flux model was employed because the time span of the numerical simulations was too short for the stratification to be affected by diurnal heating or wind-driven effects.

Numerical results (Figure 3) showed the development of strong vertically sheared flow induced by shoaling of the trough of the internal tide (distance ~ 3 km). When the crest of the succeeding internal tide shoaled (Figure 3, distance ~ 5 km), it produced an upslope propagating bore that interacted with the strong vertically sheared flow induced by the trough. The large isothermal displacement and high-frequency (higher than the tidal frequency) waves are generated around the head of the bore by the interaction of the upslope propagating bore and the downslope flows (Figure 3a). This interaction creates convergent flows on the slope near

the head of the bore (Figure 3b, distance = 4 km). The rate of turbulent kinetic energy dissipation was estimated in the SUNTANS model with the Mellor and Yamada level 2.5 turbulence closure scheme [*Mellor and Yamada*, 1982]. The numerical results indicated strong turbulent mixing in the water column around the bore head and the turbulent layer behind the bore head (distance = 6–10 km, depth = 40–50 m). The SUNTANS model reproduced the internal bores interacting with strong vertically sheared flow, consistent with the observed data shown in Figure 2.

3.2. Effects of Bottom Slope on Internal Wave Energy Dissipation

The breaking of internal gravity waves can be classified by the Iribarren number [*Boegman et al*., 2005; *Walter et al*., 2012], which is based on a similar quantity for surface gravity waves [*Iribarren and Nogales*, 1949] and is defined as

$$\xi = \frac{s}{\sqrt{a/\lambda}}, \tag{3}$$

where s is the topographic slope, a is the internal wave amplitude, and λ is the internal wavelength, such that a/λ is a measure of the internal wave steepness. Since the internal wave Froude number is given approximately by its steepness $Fr \sim a/\lambda$ [*Fringer and Street*, 2003], the Irribarren number can also be written as a ratio of the slope to the Froude number via $\xi = s\ Fr^{-1/2}$. Although numerous studies have quantified the effects of the slope and Froude number separately [*Venayagamoorthy and Fringer*, 2006; *Arthur and Fringer*, 2014], in this study we focus on the effects of the Iribarren number which has been shown to be an effective way to combine the effects of the slope and Froude number into one parameter [*Boegman et al*., 2005]. We investigated the dependence of the breaking dynamics and mixing on the Iribarren number by running the SUNTANS model with the observed Froude number ($Fr \sim 0.5$) and with six different slopes ranging from 0.46–3.4°, which gave six Iribarren numbers ($\xi = 0.20$, 0.30, 0.48, 0.71, 1.20, and 1.80). These slopes are consistent with typical slopes in the coastal ocean. The bottom slope for all cases was constant between 0 and 10 km from the left end of the domain, and the remaining 90 km was a flat bottom with a depth of 80 m. In addition to the six ξ cases, the model was run with a $\xi = 0$ case (no-slope case) to estimate internal wave energy flux with no slope reflection. Other model parameters are the same as those described in section 2.

Numerical results from two cases with $\xi = 0.2$ and 1.20 are shown in Figures 4a–4h. The numerical results from the low ξ (0.20) case showed a bore interacting with the strong tidally-driven vertically sheared flow arising from the shoaling of the internal wave trough (Figures 4a and 4c, distance ~ 6 km). The rate of turbulent kinetic energy dissipation was high around the head of the bore and along the sloping bottom (Figure 4e). For the high Iribarren number case (ξ =1.20), the vertically sheared flow induced by the shoaling internal tide trough does not last long enough to produce any significant interaction with the shoaling internal bore, and so strong breaking does not occur (Figure 4f). Although the vertical extent at which the bores run up the slope (roughly 20 m) is the same for both cases, the low bottom slope in the low ξ case leads to bore propagation that is 5 times farther up the slope than that for the high ξ case. The case with low ξ thus creates strong vertically sheared flow interacting with the bore formed by the subsequent wave, producing strong wave breaking.

The reflection coefficient (R), or the ratio of the reflected to incident internal wave energy, was estimated for the simulations by using the method described in *Venayagamoorthy and Fringer* [2006]. If all of the incoming wave energy reflects (dissipates) on the slope without (with) energy losses due to breaking, the coefficient is 1 (0). The internal wave energy was estimated at the offshore edge of the slope (distance = 10 km) and within two wave cycles after a two wave cycle spin-up. The estimated reflection coefficient increases with increasing ξ, namely, the dissipation (loss) of internal wave energy decreases with increasing ξ (Figure 4i). Strong internal wave breaking and energy dissipation is therefore limited to the runup of internal bores under low ξ conditions.

The numerical results demonstrated the relationship between the breaking and whether the internal bores were "canonical" or "noncanonical," as described by *Walter et al*. [2012] to be a strong function of the Iribarren number. For low ξ (0.20, 0.30, and 0.48) cases, waves shoal gradually over the relatively shallow slope, which results in a strong leading wave or front followed by a gradually decreasing tail or a train of rank-ordered waves (Figures 4g and 4j). Such a wave shape is termed "canonical" because open-ocean nonlinear internal gravity waves typically appear in this fashion [e.g., *Alford et al*., 2015]. For high ξ (0.71, 1.20, and 1.80) cases, waves shoal rapidly over the relatively abrupt slope, and the wave profile grows until peaking at its trailing edge to form a noncanonical bore (Figures 4h and 4j). Bottom temperature time series from the six cases clearly show a transition from a canonical bore to a noncanonical bore as a function of the Iribarren

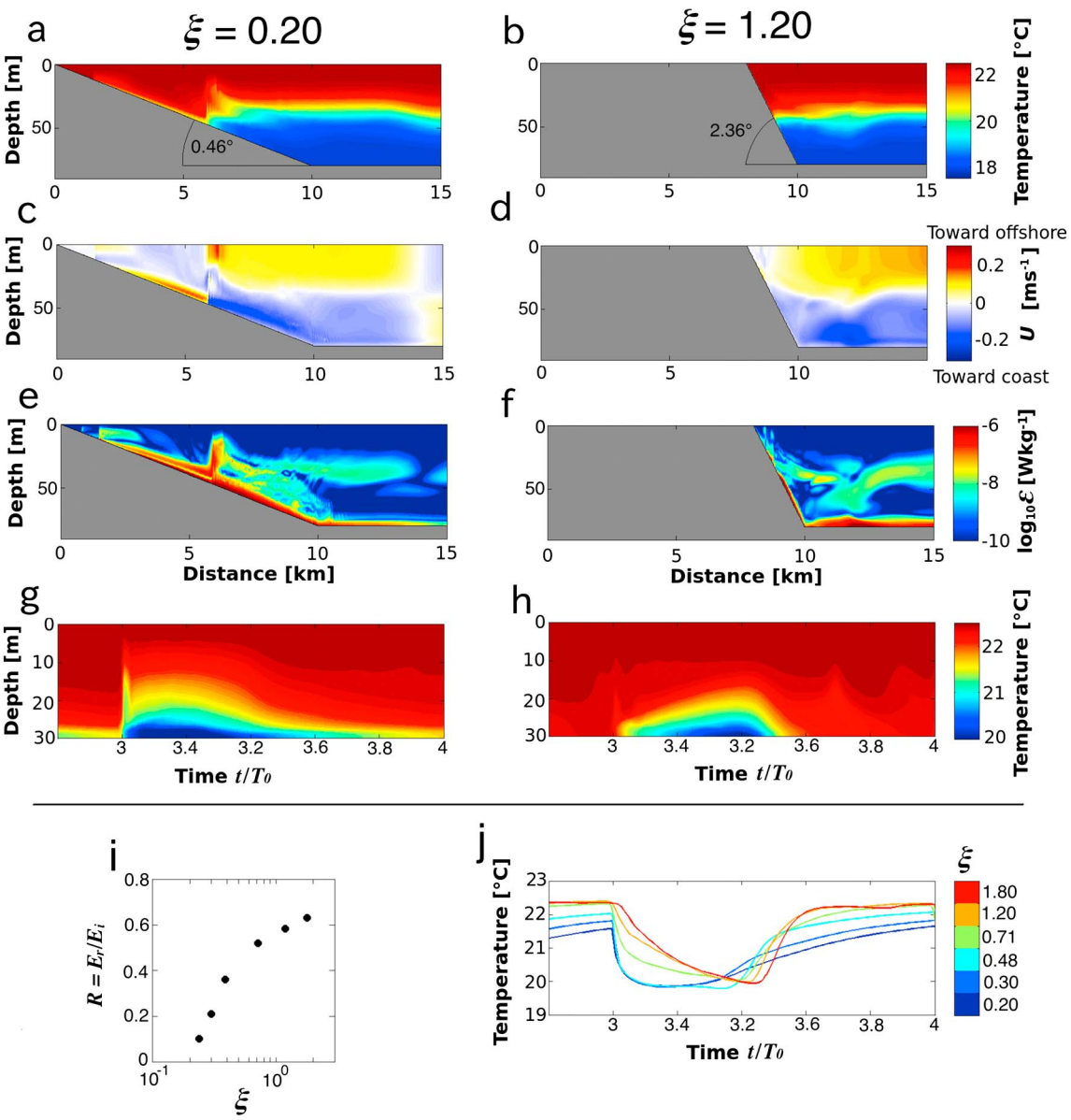

Figure 4. Numerical simulation results from the various ξ test cases, showing distributions of (a, b) temperature (c, d) horizontal currents, and (e, f) the rate of turbulent kinetic energy dissipation; (g, h) time series of temperature at 30 m depth, (i) reflection coefficient as a function of ξ, and (j) time series of bottom temperature at 30 m depth for the six simulation cases. Figures 4a, 4c, 4e, and 4g are from the $\xi = 0.20$ case and Figures 4b, 4d, 4f, and 4h are from the $\xi = 1.20$ case. The line color in Figure 4j indicates the Iribarren number. t/T_0 on Figures 4g, 4h, and 4j represents a nondimensionalized time, elapsed time (t) divided by the period of the wave (T_0).

number (Figure 4j). Strong wave breaking only occurs for canonical bores due to the strong vertically sheared flows in the trailing edge of the canonical bore interacting with the subsequent bore. Given the ubiquity of canonical wave profiles in the ocean and the dominance of shallow slopes on continental shelves, which are typically on the order of 0.5–1.0° [*Pinet*, 2011], extensive internal wave breaking is likely to occur due to the low-Iribarren number mechanism we observed in much of the coastal ocean where internal tides are present.

4. Discussion

We observed the runup of an internal bore interacting with vertically sheared flow produced by the trough of the internal tide that had just shoaled. This interaction generated enhanced wave breaking and turbulent mixing. The rate of turbulent kinetic energy dissipation reached 10^{-6}–10^{-5} W kg^{-1} near the head of the upslope propagating bore. The region of high dissipation also appeared near the sea surface above the bore

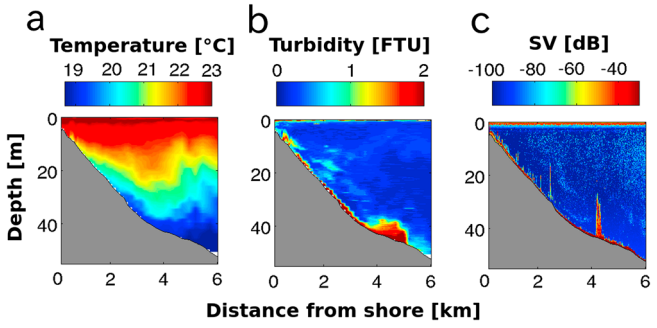

Figure 5. (a) Temperature, (b) turbidity, and (c) 125 kHz volume backscatter distributions from the transect survey.

head. Numerical simulations with the nonhydrostatic SUNTANS model reproduced the interaction of bores with the vertically sheared flows accompanied by strong downslope currents resulting in strong turbulent mixing. The simulations revealed that the Iribarren number plays a major rule in internal wave breaking mechanism. Strong mixing (wave breaking) is limited to waves in the low Iribarren number regime when canonical bore shapes produce bores that are more likely to interact with currents from subsequent shoaling internal tides. Canonical bores have been found in other bays along the east coast of Japan [*Okazaki*, 1990]. Therefore, the breaking mechanism we found is likely to significantly contribute to the total mixing this region. Based on our numerical results, the high-dissipation breaking region ($\varepsilon > 10^{-6}\,\mathrm{W\,kg^{-1}}$) extends over approximately 4% of the volume of water less than 100 m deep for the Ostuchi Bay case (Figure 3). Given that most of the coast line or bays in the region are similar to that in Ostuchi Bay with a low Iribarren number (see Figure 1b), the total volume-integrated dissipation along the coast could be roughly 40 times higher than the background dissipation level due to the internal wave breaking (assuming a background dissipation level of $10^{-9}\,\mathrm{W\,kg^{-1}}$). This implies that internal wave breaking can lead to an order of magnitude increase in the total mixing on continental shelves throughout the world's oceans.

Understanding the mechanisms of nutrient supply to continental shelves is key to understanding global ocean ecosystem dynamics [*Walsh*, 1991; *Nakatsuka et al*., 2004; *Sharples et al*., 2009]. One possible mechanism is breaking internal waves, which is thought to contribute to the cross-shelf transport of nutrients from deeper areas [*Leichter et al*., 2003] and of the resuspension and onshelf transport of sediments on continental slopes [*Cacchione et al*., 2002]. Surging of internal bores has been shown to control the distribution of fish larvae and plankton [*Pineda*, 1994]. These studies indicate that mixing events induced by internal wave breaking are essential for near-shore ocean ecosystem health. Our observations indicated the presence of strong sediment resuspension and large fish schools at the head of the bore (Figure 5, distance = 4–5 km). The sediment resuspension was likely induced by the convergent flow due to the interaction of the vertically sheared flow by the internal tide and the upslope propagating bore (the bottom shear stress exceeded the critical shear stress for fine sediments, see *Masunaga et al*. [2015] for more details). It is possible that fish gathered in the strong wave-breaking region where nutrients and phytoplankton were concentrated. This may support the idea that internal wave breaking and mixing play a role in the function of coastal ocean ecosystems.

Acknowledgments
This study was supported by funding from Tohoku Ecosystem-Associated Marine Science (TEAMS), a research program launched by the Ministry of Education, Culture, Sports, Science and Technology (MEXT). We are indebted to the crew and staff of International Coastal Research Center of the University of Tokyo. The observed data for this study are available at Research Information and data Access Site of TEAMS (RIAS, http://www.i-teams.jp/rias/).

References

Alford, M. H., et al. (2015), The formation and fate of internal waves in the South China Sea, *Nature*, *521*, 65–69.
Arthur, R. S., and O. B. Fringer (2014), The dynamics of breaking internal solitary waves on slopes, *J. Fluid Mech.*, *761*, 360–398.
Boegman, L., G. N. Ivey, and J. Imberger (2005), The degeneration of internal waves in lakes with sloping topography, *Limnol. Oceanogr.*, *50*(5), 1620–1637.
Broenkow, W. W., and S. J. McKain (1972), Tidal oscillations at the head of Monterey Submarine Canyon and their relation to oceanographic sampling and the circulation of water in Monterey Bay, in Moss Landing Marine Laboratories Technical Publication 72–5, Annual Rep., Part 6, September 1972, 42 pp., Moss Landing Marine Laboratories, Moss Landing, Calif.
Cacchione, D. A., L. F. Pratson, and A. S. Ogston (2002), The shaping of continental slopes by internal tides, *Science*, *296*, 724–727.
Carter, G. S., and M. C. Gregg (2002), Intense, variable mixing near the head of Monterey Submarine Canyon, *J. Phys. Oceanogr.*, *32*(11), 3145–3165.
Dewey, R. K., and W. R. Crawford (1988), Bottom stress estimates from vertical dissipation rate profiles on the continental shelf, *J. Phys. Oceanogr.*, *18*, 1167–1177.
Doubell, M. J., H. Yamazaki, H. Li, and Y. Kokubu (2009), An advanced laser-based fluorescence microstructure profiler (TurboMAP-L) for measuring bio-physical coupling in aquatic systems, *J. Plankton Res.*, *31*, 1441–1452.
Fringer, O. B., and R. L. Street (2003), The dynamics of breaking progressive interfacial waves, *J. Fluid Mech.*, *494*, 319–353.
Fringer, O. B., M. Gerritsen, and R. L. Street (2006), An unstructured-grid, finite-volume, nonhydrostatic, parallel coastal ocean simulator, *Ocean Model.*, *14*, 139–173.
Helfrich, K. R. (1992), Internal solitary wave breaking and run-up on a uniform slope, *J. Fluid Mech.*, *243*, 133–154.
Iribarren, C. R., and C. Nogales (1949), Protection des ports. XVIUfc Int. Congr. Navig. Lisbon, 31–80.

Leichter, J. J., H. L. Stewart, and S. L. Miller (2003), Episodic nutrient transport to Florida coral reefs, *Limnol. Oceanogr.*, *48*(4), 1394–1407.
Lemon, D., P. Johnston, J. Buermans, E. Loos, G. Borstad, and L. Brown (2012), Multiple-frequency moored sonar for continuous observations of zooplankton and fish, *Oceans*, 1–6, doi:10.1109/OCEANS.2012.6404918.
MacKinnon, J. A., and M. C. Gregg (2003), Mixing on the late-summer New England shelf—Solibores, shear, and stratification, *J. Phys. Oceanogr.*, *33*(7), 1476–1492.
Masunaga, E., and H. Yamazaki (2014), A new tow-yo instrument to observe high-resolution coastal phenomena, *J. Mar. Syst.*, *129*, 425–436.
Masunaga, E., H. Homma, H. Yamazaki, O. Fringer, T. Nagai, Y. Kitade, and A. Okayasu (2015), Mixing and sediment resuspension associated with internal bores in a shallow bay, *Cont. Shelf Res.*, *110*, 85–99.
Mellor, G. L., and T. Yamada (1982), Development of a turbulence closure model for geophysical fluid problems, *Rev. Geophys.*, *20*(4), 851–875.
Munk, W., and C. Wunsch (1998), Abyssal recipes II: Energetics of tidal and wind mixing, *Deep Sea Res., Part I*, *45*, 12.
Nakatsuka, T., M. Toda, K. Kawamura, and M. Wakatsuchi (2004), Dissolved and particulate organic carbon in the Sea of Okhotsk: Transport from continental shelf to ocean interior, *J. Geophys. Res.*, *109*, C09S14, doi:10.1029/2003JC001909.
Okazaki, M. (1990), Internal tidal waves and internal long period waves in the Sanriku coastal seas eastern coast of northern Japan, *La mer*, *28*, 5–29.
Pineda, J. (1994), Internal tidal bores in the nearshore: Warm-water fronts, seaward gravity currents and the onshore transport of neustonic larvae, *J. Mar. Res.*, *52*(3), 427–458.
Pinet, P. R. (2011), *Invitation to Oceanography*, 6th ed., Jones and Bartlett Publishers, Burlington, Mass.
Rudnick, D. L., and J. Klinke (2007), The underway conductivity-temperature-depth instrument, *J. Atmos. Oceanic Technol.*, *24*, 1910–1923.
Sharples, J., C. M. Moore, A. E. Hickman, P. M. Holligan, J. F. Tweddle, M. R. Palmer, and J. H. Simpson (2009), Internal tidal mixing as a control on continental margin ecosystems, *Geophys. Res. Lett.*, *36*, L23603, doi:10.1029/2009GL040683.
St. Laurent, L. C., and A. M. Thurnherr (2007), Intense mixing of lower thermocline water on the crest of the Mid-Atlantic Ridge, *Nature*, *448*(7154), 680–683.
Van Gastel, P., G. N. Ivey, M. J. Meuleners, J. P. Antenucci, and O. Fringer (2009), The variability of the large-amplitude internal wave field on the Australian North West Shelf, *Cont. Shelf Res.*, *29*(11), 1373–1383.
Venayagamoorthy, S. K., and O. B. Fringer (2006), Numerical simulations of the interaction of internal waves with a shelf break, *Phys. Fluids*, *18*, 076603, doi:10.1063/1.2221863.
Walsh, J. J. (1991), Importance of continental margins in the marine biogeochemical cycling of carbon and nitrogen, *Nature*, *350*, 53–55.
Walter, R. K., C. B. Woodson, R. S. Arthur, O. B. Fringer, and S. G. Monismith (2012), Nearshore internal bores and turbulent mixing in southern Monterey Bay, *J. Geophys. Res.*, *117*, C07017, doi:10.1029/2012JC008115.